

# A GPS - Integrated Slide Controller Application for Quadrotor Tracking in Straight Trajectory

**Anh Le Hoang**

Faculty of Mechanical Engineering, Vinh Long University of Technology Education, Vinh Long City, Vietnam  
anhhlh@vlute.edu.vn

**Toan Le Huu**

Faculty of Mechanical Engineering, Vinh Long University of Technology Education, Vinh Long City, Vietnam  
toanlh@vlute.edu.vn (corresponding author)

**Thuan Tran Duc**

Faculty of Mechanical Engineering, Vinh Long University of Technology Education, Hanoi, Vietnam  
thuandauto@yahoo.com

*Received: 12 September 2024 | Revised: 11 October 2024 | Accepted: 26 October 2024*

*Licensed under a CC-BY 4.0 license | Copyright (c) by the authors | DOI: <https://doi.org/10.48084/etasr.8981>*

## ABSTRACT

Unmanned Aerial Vehicle (UAV) trajectory guidance is an important area in modern aviation and automatic control, requiring the UAV to maintain precise position and velocity along the trajectory despite environmental fluctuations. This article presents the quadrotor hardware and method for developing a trajectory tracking control algorithm, using a sliding mode controller combined with GPS data. The controller's design is based on the nonlinear model of the system, integrating the nonlinear sliding mechanism with information from GPS to ensure that the system follows the target trajectory. The stability of the proposed method is proven through Lyapunov's theorem. The controller is verified through simulation and experiments. The results show that the proposed algorithm helps the quadrotor stabilize the tilt angle and track the trajectory with small errors.

**Keywords**-inertial navigation; sliding mode; drone; GPS

## I. INTRODUCTION

High-tech agriculture is an inevitable trend not only in Vietnam but also globally [1]. In the agricultural sector, Unmanned Aerial Vehicles (UAVs) are often used to perform tasks such as crop monitoring, fertilization, or pesticide spraying [2]. For spraying, the task of moving along a fixed route at a constant altitude is a fundamental problem in UAV control. Rapid advancements in network technologies, such as wireless communication, miniaturized sensors, and the Global Positioning Systems (GPS), have made UAVs valuable in both military and civilian sectors [2]. UAVs are now used in applications like aerial surveillance, precision agriculture, intelligent transportation, disaster relief, forest fire management, remote sensing, and traffic monitoring [3]. Their affordability, maneuverability, and efficient deployment contribute to their widespread adoption [4]. UAVs are classified by size, payload, range, battery life, altitude, and flight dynamics [5, 6]. Navigation relies on sensors such as GPS, accelerometers, gyroscopes, and Inertial Navigation System (INS), though INS accuracy may suffer from integral

drift errors [7]. GPS systems provide global coverage, high precision, and cost-effectiveness for outdoor navigation. Authors in [8] proposed a feedback controller for automating UAV takeoff and landing using IMU and GPS data with a Kalman filter [8]. GPS, or Satellite-based Navigation Systems (SNSs), are effective for 3D positioning of UAVs, 3D Indoor reconstruction from photogrammetry, Unmanned Ground Vehicles (UGVs), and autonomous underwater vehicles [9]. Authors in [10, 11] demonstrated that Differential GPS (DGPS) improves positioning accuracy by mitigating errors from satellite clock, position, and signal delay, with further improvements achieved by integrating DGPS with a single antenna receiver. Although GPS alone can estimate the position of a vehicle, it is often prone to errors due to weak signals and satellite interference, resulting in loss of positioning data. GPS data are often integrated with information from other sensors, the most common being the GPS/INS method, which combines data from INS and GPS to reduce errors and improve positioning accuracy [12]. Authors in [13] used a Kalman filter to fuse data from GPS with INS information. This algorithm, although tested on ground vehicles, is also applicable to UAVs.

UAV trajectories are usually straight or circular, with the requirement to maintain accuracy and stability against interference effects. Trajectory tracking algorithms, nonlinear guidance [14], vector field-based guidance [15], linear quadrature correction [16], pursuit, and line-of-sight tracking [17], have been developed to address this problem.

II. HARDWARE STRUCTURE

The Quadrotor (Figure 1) is a popular UAV in education and research due to its affordability, durability, and reliability in both indoor and outdoor environments. Constructed of carbon fiber and plastic, the device is equipped with a battery, four BLDC motors, and a 6-degree-of-freedom inertial measurement unit. Parameters such as yaw, altitude, vertical speed, and motor speed can be adjusted via the control panel. The Quadrotor is capable of speeds exceeding 4 m/s and has a flight time of approximately 10 minutes.



Fig. 1. Quadrotor UAV.

The Quadrotor is controlled by the Pixhawk processor, equipped with a 32-bit ARM Cortex M4 core with an FPU operating at 168 MHz. The control system connects the Pixhawk to the Jetson board and uses GPS for positioning as well as developing the trajectory tracking algorithm. The main components include:

GPS Module: Provides positioning data.

- Drone Frame: Includes the motor and the ESC (Electronic Speed Controller).
- Controller: Includes Transmitter and Receiver.
- Batteries and Accessories: Provide necessary power and connections.
- Jetson Nano: The onboard computer processes flight control algorithms and transmits commands to the Pixhawk via UART or I2C protocol.
- Pixhawk: The flight controller executes commands from the Jetson, controlling the motors, propellers and sensors to perform the programmed trajectory.

The quadrotor's operating procedure in orbit tracking (Figure 2) is divided into three main stages: (1) take-off, (2) orbit tracking, and (3) landing.

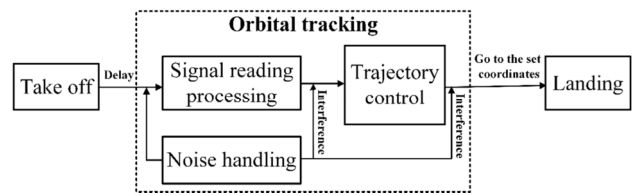


Fig. 2. Quadrotor orbit tracking process diagram.

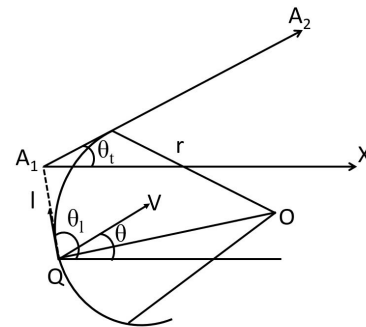


Fig. 3. Quadrotor orbit tracking state diagram.

III. PATH FOLLOWING ALGORITHM

The kinematic modeling problem is approached as follows: Given a trajectory with the UAV position at M (x, y) and an angle of orientation  $\theta$ , the objective is to determine the optimal angle of orientation for the UAV to move and follow the trajectory. The trajectory is modeled by straight lines, each segment is defined by a sequence of landmarks and the angle between the segments connecting consecutive points.

Below is a guidance algorithm using intermittent signals, developed based on the diagram in Figure 3, with the Quadrotor following the path connecting two points  $A_1$  and  $A_2$ . The quadrotor motion equation is described by:

$$\begin{cases} \dot{l} = v \cdot \sin(\theta - \theta_i) \\ \dot{\theta} = k \cdot u \end{cases} \quad (1)$$

where  $l$  is the distance from the quadrotor to the trajectory,  $\theta$  is the angular error of the quadrotor and the trajectory angle,  $v$  is the velocity,  $u = \tan \Delta$  is the control signal,  $\Delta$  is the tilt angle of the UAV, and the radius of the orbit is  $r = v/\omega$  where  $\omega$  is the maximum rotation speed (rad/s).

The trajectory connecting the two points  $A_1(la_1, lo_1), A_2(la_2, lo_2)$  is determined by:

$$\begin{aligned} \Delta la &= la_2 - la_1 \\ \Delta lo &= lo_2 - lo_1 \end{aligned} \quad (2)$$

with:

$$\begin{aligned} a &= lo_2 - lo_1 \\ b &= la_2 - la_1 \\ c &= la_2 \cdot lo_1 - la_1 \cdot lo_2 \end{aligned}$$

Convert to radians:

$$dLa = \Delta la \cdot \frac{\pi}{180}$$

$$dLo = \Delta lo \cdot \frac{\pi}{180} \cdot \cos\left(la_1 \cdot \frac{\pi}{180}\right) \quad (3)$$

The distance between the two points is:

$$D = \sqrt{(dLa \cdot Er)^2 + (dLo \cdot Er)^2} \quad (4)$$

where  $la$  is the position of the point along the  $x$ -axis,  $lo$  is the position of the point along the  $y$ -axis,  $Er$  is the radius of the earth (6378137(m)), and  $D$  is the distance (m).

Since the trajectory is a straight line with directions from  $A_1$  and  $A_2$ , the angle of the trajectory is determined in the entire plane, thus:

$$\theta_t = \arctan2((lo_2 - lo_1), (la_2 - la_1)) \quad (5)$$

The coordinates of the quadrotor are determined as  $Q(x_u, y_u)$ .

The distance from the Quadrotor to  $A_1A_2$  is determined by:

$$l = \left(-\frac{a \cdot x_u + c}{b} - y_u\right) \cdot \cos \theta_t \quad (6)$$

According to the Dubin orbit, the relationship between  $\theta_t$  and  $l$  is defined as follows:

$$\begin{cases} \theta_t = -\frac{\pi}{2} \text{sign}l + \theta_t & \text{when } |l| > r \\ \theta_t = -\left(\frac{\pi}{2} - \arcsin\left(1 - \frac{|l|}{r}\right)\right) \text{sign}l + \theta_t & |l| \leq r \end{cases} \quad (7)$$

From (2) and (1), we see that the distance from  $Q$  to the orbit  $l$  is replaced by the horizontal position error denoted by  $e$  (saturation function):

$$\begin{cases} e = r & \text{when } |l| > r \\ e = d & |l| \leq r \end{cases} \quad (8)$$

Equation (7) is rewritten as:

$$N = \theta_t - \theta_i = -\left(\frac{\pi}{2} - \arcsin\left(1 - \frac{|e|}{r}\right)\right) \text{sign}e \quad (9)$$

Equation (4) can be used to construct the nonlinear sliding surface. Then, for system (1), the sliding mode with sliding surface (10) will be used:

$$s = N + \text{sign}e \left[ \frac{\pi}{2} - \arcsin\left(1 - \frac{e \cdot \text{sign}e}{r}\right) \right] \quad (10)$$

and:

$$\dot{s} = \dot{\theta}_t - \dot{\theta}_i + \text{sign}e \left( \frac{1}{\sqrt{\frac{2|e|}{r} - \frac{|e|^2}{r^2}}} \cdot \frac{\gamma}{r} \cdot \text{sign}e \cdot \sin N \right) \quad (11)$$

The chosen Lyapunov function is:

$$T_1 = 0.5s^2 \quad (12)$$

Taking the derivative  $\dot{T}_1 = s \cdot \dot{s}$  and from (11) we have:

$$\dot{T}_1 = s \left( \dot{\theta}_t - \dot{\theta}_i + \text{sign}e \left( \frac{1}{\sqrt{\frac{2|e|}{r} - \frac{|e|^2}{r^2}}} \cdot \frac{\gamma}{r} \cdot \text{sign}e \cdot \sin N \right) \right) \quad (13)$$

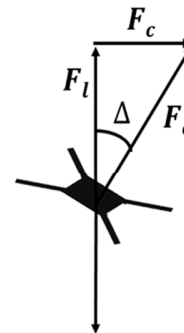


Fig. 4. Quadrotor angle velocity determination diagram.

The forces acting on the quadrotor are: gravity ( $F_g$ ), with  $m$  being the UAV mass, the lift force ( $F_l$ ), the centripetal force of the rotation of the UAV ( $F_c$ ), and the aerodynamic force ( $F_e$ ), with  $F_l = F_g$ . Then:

$$\begin{cases} F_e \cdot \cos \Delta = F_g = m \cdot g \\ F_e \cdot \sin \Delta = F_c = \frac{m \cdot \gamma^2}{r} \end{cases} \quad (14)$$

From (14) we get:

$$\tan \Delta = \frac{\gamma^2}{r \cdot g} = \dot{\theta}_t \cdot \frac{\gamma}{g} \quad (15)$$

Or:

$$\dot{\theta}_t = \frac{g}{\gamma} \cdot u \quad (16)$$

There is a sliding mode with the control command:

$$u = \frac{\gamma}{g} \left( \left( \dot{\theta}_t - \frac{1}{\sqrt{\frac{2|e|}{r} - \frac{|e|^2}{r^2}}} \cdot \frac{\gamma}{r} \cdot \sin N \right) - \delta \cdot \text{sign} s \right) \quad (17)$$

Putting (16) and (13) into (17), we get:

$$\dot{T}_1 = s \begin{pmatrix} \dot{\theta}_i - \dot{\theta}_i + \frac{1}{\sqrt{1 - \left(1 - \frac{|e|}{r}\right)^2}} \cdot \frac{\gamma}{r} \cdot \sin N \\ - \frac{1}{\sqrt{1 - \left(1 - \frac{|e|}{r}\right)^2}} \cdot \frac{\gamma}{r} \cdot \sin N - \delta \cdot \text{sign} s \end{pmatrix} \quad (18)$$

which is an asymptotically stable system. The chosen Lyapunov function becomes:

$$T_2 = 0.5[N^2 + e^2] \quad (19)$$

Taking the derivative of  $T_2$  and using (1), (8), and (9) we get:

$$\begin{aligned} \dot{T}_2 &= N \left[ -\text{sign} e \left( -\frac{1}{\sqrt{\frac{2|e|}{r} - \frac{|e|^2}{r^2}}} \cdot \frac{1}{r} \cdot \text{sign} e \cdot \gamma \cdot \sin N \right) \right. \\ &\quad \left. + e \cdot \gamma \cdot \sin N \right] \quad (20) \\ &= -\frac{1}{\sqrt{\frac{2|e|}{r} - \frac{|e|^2}{r^2}}} \cdot \frac{\gamma}{r} \cdot N \cdot \sin N + |e| \cdot \text{sign} e \cdot \gamma \cdot \sin N \end{aligned}$$

From (9) we see that:

$$\text{sign} N = -\text{sign} e \quad (21)$$

Besides:

$$N = |N| \text{sign} N \quad (22)$$

Equation (2) is re-written with the help of (21), (22), as:

$$T_2 = - \left( \frac{1}{\sqrt{\frac{2|e|}{r} - \frac{|e|^2}{r^2}}} \cdot \frac{\gamma}{r} \cdot |N| + |e| \right) \cdot \sin N \cdot \text{sign} N \quad (23)$$

From (9) we have:

$$-\pi/2 \leq \theta_i - \theta_i \leq \pi/2 \quad (24)$$

In the interval  $[-\pi/2; \pi/2]$ ,  $\sin x$  and  $x$  are increasing, so:

$$\sin N = |\sin N| \cdot \text{sign} N \quad (25)$$

Putting (19) into (17) we have:

$$\dot{T}_2 = - \left( \frac{1}{\sqrt{\frac{2|e|}{r} - \frac{|e|^2}{r^2}}} \cdot \frac{\gamma}{r} \cdot |N| + |e| \right) \cdot |\sin N| < 0 \quad (26)$$

From (26) it can be seen that  $\dot{T}_2 < 0$  and that when operating in sliding mode the system will be asymptotically stable.

#### IV. EXPERIMENTAL RESULTS

The implementation process applied to the experimental model and controlling it to fly along a straight trajectory between two determined points follows: Use formula (2) to calculate the distance between the two points, then convert the value to radians according to (3), and finally apply (4) to determine the exact distance between the two points.

Flight Test 1:

$$A_1 (10.250546006300228; 105.96175657854099)$$

$$A_2 (10.2504098802617; 105.961759458414)$$

$$D_1 = 15.504$$

Flight test 2:

$$A_1 (10.250546006300228; 105.96175657854099)$$

$$A_2 (10.2504039416131; 105.961756776205)$$

$$D_2 = 15.814$$

Flight Test 3:

$$A_1 (10.250546006300228; 105.96175657854099)$$

$$A_2 (10.2503975401149; 105.961759260749)$$

$$D_3 = 16.791$$

Flight Test 4:

$$A_1 (10.250546006300228; 105.96175657854099)$$

$$A_2 (10.2503953635649; 105.961757446757)$$

$$D_4 = 16.769$$

Flight Test 5:

$$A_1 (10.250546006300228; 105.96175657854099)$$

$$A_2 (10.250394283607; 105.961755744337)$$

$$D_5 = 16.889$$

Figures 5 and 6 demonstrate that the quadrotor's flight trajectory closely matches the designated flight path, demonstrating accurate trajectory tracking performance. Specifically, Figure 5 depicts the quadrotor's compliance with the designated trajectory, while Figure 6 provides a detailed view of how the actual trajectory matches the intended path according to the set distance. In addition, Figure 7 presents the

tilt angles in the X and Y directions during trajectory tracking. The data in Figure 7 show that these tilt angles exhibit minimal deviation, emphasizing the accuracy of the quadrotor's orientation control capability during flight.

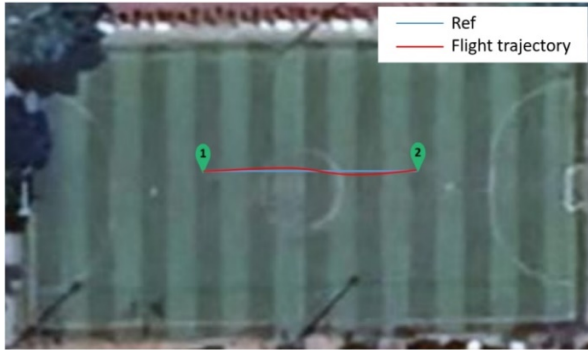


Fig. 5. Flight trajectory.

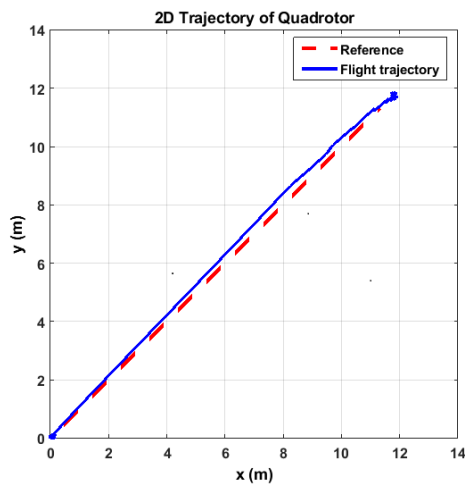


Fig. 6. Flight test 1 trajectory in simulation.

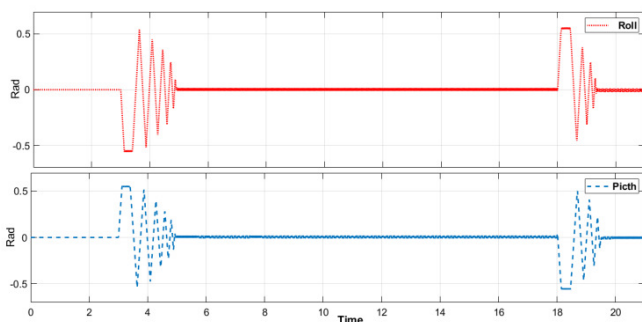


Fig. 7. Roll angle and pitch angle.

To determine the quadrotor average error we use the RMSE formula:

$$RMSE = \sqrt{\frac{1}{n} \sum_{a=1}^n (\tau_a - \lambda_a)^2} \tag{27}$$

where  $\tau_a$  is the value set at position,  $\lambda_a$  is the actual value, and  $n$  is the total number of pairs of set and actual values.

The experimental data indicate that the deviation between the set and actual distances remains within acceptable limits, with a trajectory error rate ranging from 1.21% to 1.39%. The RMSE (Root Mean Square Error) index of the  $La$  and  $Lo$  measurement methods demonstrate high accuracy, with RMSE values ranging from 2.07E-06 to 3.77E-07. The research findings confirm that integrating GPS with a sliding control algorithm enhances both the accuracy and stability of the UAV system during trajectory tracking. Furthermore, experimental results validate the system's effectiveness, evidenced by low trajectory error, minimal RMSE values, and reliable performance in outdoor conditions.

TABLE I. FLIGHT TEST RESULTS

Order	Setting distance	Actual distance	Orbital error	RMSE $La$	RMSE $Lo$
1	15.504	15.714	1.34%	2.12E-06	3.21E-07
2	15.814	16.037	1.39%	2.07E-06	3.67E-07
3	16.791	16.997	1.21%	2.28E-06	3.77E-07
4	16.769	16.985	1.27%	2.15E-06	3.11E-07
5	16.889	17.112	1.30%	2.09E-06	3.45E-07

### V. CONCLUSION

The experimental results show that the control algorithm based on nonlinear sliding mode combined with GPS data helps the quadrotor system achieve rapid stabilization. This algorithm not only enhances the ability to maintain stability but also improves the efficiency of tracking the pre-set trajectory. After five tests with different coordinates, small errors in distance were recorded, confirming the effectiveness of the proposed method. In the context of the development of control technology applications, especially in autonomous and unmanned aerial systems, it is necessary to prepare for situations where the GPS signal is damaged or weakened.

### REFERENCES

- [1] N. M. Elfatih, E. S. Ali, and R. A. Saeed, "Navigation and Trajectory Planning Techniques for Unmanned Aerial Vehicles Swarm," in *Artificial Intelligence for Robotics and Autonomous Systems Applications*, A. T. Azar and A. Koubaa, Eds. New York, NY, USA: Springer, 2023, pp. 369–404.
- [2] Y. Wang *et al.*, "Trajectory Design for UAV-Based Internet of Things Data Collection: A Deep Reinforcement Learning Approach," *IEEE Internet of Things Journal*, vol. 9, no. 5, pp. 3899–3912, Mar. 2022, <https://doi.org/10.1109/JIOT.2021.3102185>.
- [3] B. Syd Ali, "Traffic management for drones flying in the city," in *22nd Air Transport Research Society (ATRS) World Conference*, Seoul, South Korea, Jul. 2018, vol. 26, pp. 1–11, <https://doi.org/10.1016/j.jijcip.2019.100310>.
- [4] S. A. H. Mohsan, N. Q. H. Othman, Y. Li, M. H. Alsharif, and M. A. Khan, "Unmanned aerial vehicles (UAVs): practical aspects, applications, open challenges, security issues, and future trends," *Intelligent Service Robotics*, vol. 16, no. 1, pp. 109–137, Mar. 2023, <https://doi.org/10.1007/s11370-022-00452-4>.
- [5] O. Tachinina, A. Lysenko, and V. Kutieпов, "Classification of Modern Unmanned Aerial Vehicles," *Electronics and Control Systems*, vol. 4, no. 74, pp. 79–86, Dec. 2022, <https://doi.org/10.18372/1990-5548.74.17354>.

- [6] F. Alotaibi, A. Al-Dhaqm, and Y. D. Al-Otaibi, "A Conceptual Digital Forensic Investigation Model Applicable to the Drone Forensics Field," *Engineering, Technology & Applied Science Research*, vol. 13, no. 5, pp. 11608–11615, Oct. 2023, <https://doi.org/10.48084/etasr.6195>.
- [7] J. Kwak and Y. Sung, "Autonomous UAV Flight Control for GPS-Based Navigation," *IEEE Access*, vol. 6, pp. 37947–37955, Jan. 2018, <https://doi.org/10.1109/ACCESS.2018.2854712>.
- [8] N. Sedlmair, J. Theis, and F. Thielecke, "Flight Testing Automatic Landing Control for Unmanned Aircraft Including Curved Approaches," *Journal of Guidance, Control, and Dynamics*, vol. 45, no. 4, pp. 726–739, 2022, <https://doi.org/10.2514/1.G005917>.
- [9] J. Gross *et al.*, "Field-Testing of a UAV-UGV Team for GNSS-Denied Navigation in Subterranean Environments," in *32nd International Technical Meeting of the Satellite Division of The Institute of Navigation*, Miami, FL, USA, Sep. 2019, pp. 2112–2124, <https://doi.org/10.33012/2019.16912>.
- [10] B. Grayson, N. T. Penna, J. P. Mills, and D. S. Grant, "GPS precise point positioning for UAV photogrammetry," *The Photogrammetric Record*, vol. 33, no. 164, pp. 427–447, 2018, <https://doi.org/10.1111/phor.12259>.
- [11] J. Kim *et al.*, "Accuracy Improvement of DGPS for Low-Cost Single-Frequency Receiver Using Modified Flächen Korrektur Parameter Correction," *ISPRS International Journal of Geo-Information*, vol. 6, no. 7, Jul. 2017, Art. no. 222, <https://doi.org/10.3390/ijgi6070222>.
- [12] J. H. Ryu, G. Gankhuyag, and K. T. Chong, "Navigation System Heading and Position Accuracy Improvement through GPS and INS Data Fusion," *Journal of Sensors*, vol. 2016, no. 1, 2016, Art. no. 7942963, <https://doi.org/10.1155/2016/7942963>.
- [13] L. Hu, J. Wang, S. Wang, and H. Cui, "Processing and Analysis of Multi-antenna GNSS/INS Fully Combined Model," in *China Satellite Navigation Conference*, Beijing, China, Dec. 2022, pp. 255–264, [https://doi.org/10.1007/978-981-19-2588-7\\_24](https://doi.org/10.1007/978-981-19-2588-7_24).
- [14] S. Berkane, A. Tayebi, and S. de Marco, "A nonlinear navigation observer using IMU and generic position information," *Automatica*, vol. 127, May 2021, Art. no. 109513, <https://doi.org/10.1016/j.automatica.2021.109513>.
- [15] W. Yao, H. G. de Marina, B. Lin, and M. Cao, "Singularity-Free Guiding Vector Field for Robot Navigation," *IEEE Transactions on Robotics*, vol. 37, no. 4, pp. 1206–1221, Dec. 2021, <https://doi.org/10.1109/TRO.2020.3043690>.
- [16] F. von Frankenberg and S. B. Nokleby, "Inclined landing testing of an omni-directional unmanned aerial vehicle," *Transactions of the Canadian Society for Mechanical Engineering*, vol. 42, no. 1, pp. 61–70, Mar. 2018, <https://doi.org/10.1139/tcsme-2017-0008>.
- [17] J. T. Hing, K. W. Sevcik, and P. Y. Oh, "Development and Evaluation of a Chase View for UAV Operations in Cluttered Environments," *Journal of Intelligent and Robotic Systems*, vol. 57, no. 1, pp. 485–503, Jan. 2010, <https://doi.org/10.1007/s10846-009-9356-4>.